Eur. Phys. J. C 16, 139–153 (2000)
Digital Object Identifier (DOI) 10.1007/s100520000404

THE EUROPEAN PHYSICAL JOURNAL C

Decay widths of the neutral $\mathcal{CP}$-even MSSM Higgs bosons in the Feynman-diagrammatic approach

S. Heinemeyer[1,a], W. Hollik[2,b], G. Weiglein[3,c]

[1] DESY Theorie, Notkestrasse 85, 22603 Hamburg, Germany
[2] Institut für Theoretische Physik, Universität Karlsruhe, 76128 Karlsruhe, Germany
[3] CERN, TH Division, 1211 Geneva 23, Switzerland

Received: 9 March 2000 / Published online: 14 April 2000 – © Springer Verlag 2000

Abstract. In the Minimal Supersymmetric Standard Model (MSSM) we incorporate the Higgs-boson propagator corrections, evaluated up to two-loop order, into the prediction of $\Gamma(h \to f\bar{f})$ and $BR(h \to f\bar{f})$ for $f = b, c, \tau$. The propagator corrections consist of the full one-loop contribution, including the effects of non-vanishing external momentum, and corrections of $\mathcal{O}(\alpha\alpha_s)$ at the two-loop level. The results are supplemented with the dominant one-loop QED corrections and final state QCD corrections from both gluons and gluinos. The effects of the two-loop propagator corrections and of the one-loop gluino contributions are investigated in detail. Our results are compared with the result obtained within the renormalization group approach. Agreement within 10% is found for most parts of the MSSM parameter space.

1 Introduction

The search for the lightest Higgs boson is a crucial test of Supersymmetry (SUSY) that can be performed with the present and the next generation of accelerators. The prediction of a relatively light Higgs boson is common to all supersymmetric models whose couplings remain in the perturbative regime up to a very high energy scale [1]. Finding the Higgs boson is thus one of the main goals of todays high-energy physics. Concerning the Higgs boson search, it is necessary to know the decay widths and branching ratios of the main decay channels to a high accuracy. After the detection of a scalar particle it is mandatory as a next step to measure its couplings to gauge bosons and fermions and also its self-couplings very accurately, in order to establish the Higgs mechanism and the Yukawa interactions experimentally. The determination of the trilinear Higgs-boson self-couplings might be possible at a future linear e^+e^- collider with high luminosity [2].

In this paper we concentrate on the coupling of the lightest MSSM Higgs boson to Standard model (SM) fermions. In the MSSM the mass of the lightest Higgs boson, m_h, is bounded from above by $m_h \lesssim 135$ GeV, including radiative corrections up to two-loop order [3–11]. Since the b-, the c-quark and the τ-lepton are the heaviest particles for which the decay $h \to f\bar{f}$ is kinematically allowed, it is of particular interest to calculate their corresponding decay rates and branching ratios with high precision [12–18]. We analyze these decay rates and branching ratios, taking into account the Higgs-boson propagator corrections, where at the one-loop level the full momentum dependence is kept. These corrections contain the Yukawa contributions of $\mathcal{O}(G_F m_t^4/M_W^2)$, which are the dominant electroweak one-loop corrections to the Higgs-boson decay width, and the corresponding QCD corrections of $\mathcal{O}(G_F \alpha_s m_t^4/M_W^2)$ as well as the Yukawa corrections of $\mathcal{O}(G_F^2 m_t^6/M_W^2)$. We also take into account the one-loop vertex corrections resulting from gluon, gluino and photon exchange together with real gluon and photon emission as given in [12]. Only the purely weak $\mathcal{O}(\alpha)$ vertex corrections have been neglected. We numerically investigate the effect of the two-loop propagator contributions and the one-loop gluino-exchange vertex correction. The latter one has been mostly neglected in experimental analyses so far, but can have a large impact on the result. We show analytically that the Higgs-boson propagator correction with neglected momentum dependence can be absorbed into the tree-level coupling using the effective mixing angle from the neutral $\mathcal{CP}$-even Higgs boson sector. The result in this approximation is then compared with the full result. We also perform a comparison between our full result and the renormalization group (RG) improved effective potential calculation, see [19] and references therein. For most parts of the MSSM parameter space we find agreement within 10% between the two approaches, although deviations up to 50% are possible for certain ranges of the parameter space.

The paper is organized as follows: in Sect. 2 we give the calculational basis needed for the incorporation of the two-loop Higgs-propagator corrections into the decay widths. We show analytically how the propagator corrections with

[a] e-mail: Sven.Heinemeyer@desy.de
[b] e-mail: Wolfgang.Hollik@physik.uni-karlsruhe.de
[c] e-mail: Georg.Weiglein@cern.ch

neglected external momentum are related to the effective mixing-angle approach. The results for the gluon, gluino and QED vertex corrections in combination with gluon and photon bremsstrahlung are reviewed. In Sect. 3 a numerical analysis for the decay rates and a comparison of the full result and the effective mixing-angle result is performed. Special emphasis is put on the two-loop propagator correction and the one-loop gluino contribution. Section 4 contains the comparison of our full result with the RG approach. The conclusions can be found in Sect. 5.

2 Calculational basis

The Higgs potential of the MSSM is given by [20]

$$V = m_1^2 H_1 \bar{H}_1 + m_2^2 H_2 \bar{H}_2 - m_{12}^2(\epsilon_{ab} H_1^a H_2^b + \text{h.c.}) + \frac{g'^2+g^2}{8}(H_1\bar{H}_1 - H_2\bar{H}_2)^2 + \frac{g^2}{2}|H_1\bar{H}_2|^2, \quad (1)$$

where m_1, m_2, m_{12} are soft SUSY-breaking terms, g, g' are the $SU(2)$ and $U(1)$ gauge couplings, and $\epsilon_{12} = -1$. The doublet fields H_1 and H_2 are decomposed in the following way:

$$H_1 = \begin{pmatrix} H_1^1 \\ H_1^2 \end{pmatrix} = \begin{pmatrix} v_1 + (\phi_1^0 + i\chi_1^0)/\sqrt{2} \\ \phi_1^- \end{pmatrix},$$
$$H_2 = \begin{pmatrix} H_2^1 \\ H_2^2 \end{pmatrix} = \begin{pmatrix} \phi_2^+ \\ v_2 + (\phi_2^0 + i\chi_2^0)/\sqrt{2} \end{pmatrix}. \quad (2)$$

Besides g and g', two independent parameters enter the potential (1): $\tan\beta = v_2/v_1$ and $M_A^2 = -m_{12}^2(\tan\beta + \cot\beta)$, where M_A is the mass of the $\mathcal{CP}$-odd A boson.

The $\mathcal{CP}$-even neutral mass eigenstates are obtained performing the rotation

$$\begin{pmatrix} H^0 \\ h^0 \end{pmatrix} = \begin{pmatrix} \cos\alpha & \sin\alpha \\ -\sin\alpha & \cos\alpha \end{pmatrix} \begin{pmatrix} \phi_1^0 \\ \phi_2^0 \end{pmatrix} \equiv D^{-1}(\alpha) \begin{pmatrix} \phi_1^0 \\ \phi_2^0 \end{pmatrix} \quad (3)$$

with the mixing angle α related to $\tan\beta$ and M_A by

$$\tan 2\alpha = \tan 2\beta \frac{M_A^2 + M_Z^2}{M_A^2 - M_Z^2}, \quad -\frac{\pi}{2} < \alpha < 0. \quad (4)$$

At the tree level the mass matrix of the neutral $\mathcal{CP}$-even Higgs bosons in the ϕ_1, ϕ_2 basis can be expressed in terms of M_Z and M_A as follows:

$$M_{\text{Higgs}}^{2,\text{tree}} = \begin{pmatrix} m_{\phi_1}^2 & m_{\phi_1\phi_2}^2 \\ m_{\phi_1\phi_2}^2 & m_{\phi_2}^2 \end{pmatrix} \quad (5)$$
$$= \begin{pmatrix} M_A^2 \sin^2\beta + M_Z^2 \cos^2\beta & -(M_A^2 + M_Z^2)\sin\beta\cos\beta \\ -(M_A^2 + M_Z^2)\sin\beta\cos\beta & M_A^2\cos^2\beta + M_Z^2\sin^2\beta \end{pmatrix}.$$

Transforming to the eigenstate basis (3) yields

$$M_{\text{Higgs}}^{2,\text{tree}} \xrightarrow{\alpha} \begin{pmatrix} m_H^2 & 0 \\ 0 & m_h^2 \end{pmatrix} \quad (6)$$

with m_h and m_H being the tree-level masses of the neutral $\mathcal{CP}$-even Higgs bosons.

In the Feynman diagrammatic (FD) approach the higher-order corrected Higgs boson masses, denoted by M_h, M_H, are derived by finding the poles of the h, H-propagator matrix whose inverse is given by

$$(\Delta_{\text{Higgs}})^{-1} = -i \begin{pmatrix} q^2 - m_H^2 + \hat{\Sigma}_H(q^2) & \hat{\Sigma}_{hH}(q^2) \\ \hat{\Sigma}_{hH}(q^2) & q^2 - m_h^2 + \hat{\Sigma}_h(q^2) \end{pmatrix}, \quad (7)$$

where the $\hat{\Sigma}(q^2)$ denote the renormalized Higgs boson self-energies. For these self-energies we take the result up to two-loop order, see Sect. 2.2 below.

Our main emphasis in this paper is on the fermionic decays of the light Higgs boson, but for completeness we list the expressions for both h and H. The amplitudes for the decays $h, H \to f\bar{f}$ can be written as follows:

$$A(h \to f\bar{f}) = \sqrt{Z_h}\,(\Gamma_h + Z_{hH}\,\Gamma_H)\ , \quad (8)$$
$$A(H \to f\bar{f}) = \sqrt{Z_H}\,(\Gamma_H + Z_{Hh}\,\Gamma_h)\ , \quad (9)$$

with

$$Z_{hH} = -\frac{\hat{\Sigma}_{hH}(M_h^2)}{M_h^2 - m_H^2 + \hat{\Sigma}_H(M_h^2)}, \quad (10)$$
$$Z_{Hh} = -\frac{\hat{\Sigma}_{hH}(M_H^2)}{M_H^2 - m_h^2 + \hat{\Sigma}_h(M_H^2)}, \quad (11)$$

involving the renormalized self-energies $\hat{\Sigma}(q^2)$ and 3-point vertex functions Γ_h, Γ_H. The wave function renormalization factors Z_h and Z_H are related to the finite residues of the h and H propagators, respectively:

$$Z_h = \frac{1}{1 + \text{Re}\,\hat{\Sigma}_h'(q^2) - \text{Re}\left(\frac{\hat{\Sigma}_{hH}^2(q^2)}{q^2 - m_H^2 + \hat{\Sigma}_H(q^2)}\right)'}\Bigg|_{q^2=M_h^2} \quad (12)$$

$$Z_H = \frac{1}{1 + \text{Re}\,\hat{\Sigma}_H'(q^2) - \text{Re}\left(\frac{\hat{\Sigma}_{hH}^2(q^2)}{q^2 - m_h^2 + \hat{\Sigma}_h(q^2)}\right)'}\Bigg|_{q^2=M_H^2}. \quad (13)$$

2.1 The α_{eff}-approximation

The dominant contributions for the Higgs boson self-energies can be obtained by setting $q^2 = 0$. Approximating the renormalized Higgs boson self-energies by

$$\hat{\Sigma}(q^2) \to \hat{\Sigma}(0) \equiv \hat{\Sigma} \quad (14)$$

yields the Higgs boson masses by re-diagonalizing the dressed mass matrix

$$M_{\text{Higgs}}^2 = \begin{pmatrix} m_H^2 - \hat{\Sigma}_H & -\hat{\Sigma}_{hH} \\ -\hat{\Sigma}_{hH} & m_h^2 - \hat{\Sigma}_h \end{pmatrix} \xrightarrow{\Delta\alpha} \begin{pmatrix} M_H^2 & 0 \\ 0 & M_h^2 \end{pmatrix}, \quad (15)$$

where M_h and M_H are the corresponding higher-order-corrected Higgs boson masses. The rotation matrix in the transformation (15) reads:

$$D(\Delta\alpha) = \begin{pmatrix} \cos\Delta\alpha & -\sin\Delta\alpha \\ \sin\Delta\alpha & \cos\Delta\alpha \end{pmatrix} . \tag{16}$$

The angle $\Delta\alpha$ is related to the renormalized self-energies and masses through the eigenvector equation

$$\begin{pmatrix} m_H^2 - \hat{\Sigma}_H - M_h^2 & -\hat{\Sigma}_{hH} \\ -\hat{\Sigma}_{hH} & m_h^2 - \hat{\Sigma}_h - M_h^2 \end{pmatrix} \begin{pmatrix} -\sin\Delta\alpha \\ \cos\Delta\alpha \end{pmatrix} = 0 \tag{17}$$

which yields

$$\frac{\hat{\Sigma}_{hH}}{M_h^2 - m_H^2 + \hat{\Sigma}_H} = \tan\Delta\alpha . \tag{18}$$

The second eigenvector equation leads to:

$$\frac{-\hat{\Sigma}_{hH}}{M_H^2 - m_h^2 + \hat{\Sigma}_h} = \tan\Delta\alpha . \tag{19}$$

With the approximation (14) one deduces

$$Z_{hH} = -\frac{\hat{\Sigma}_{hH}}{M_h^2 - m_H^2 + \hat{\Sigma}_H} = -\tan\Delta\alpha, \tag{20}$$

$$Z_{Hh} = -\frac{\hat{\Sigma}_{hH}}{M_H^2 - m_h^2 + \hat{\Sigma}_h} = +\tan\Delta\alpha, \tag{21}$$

and Z_h can be expressed as

$$\begin{aligned} Z_h &= \frac{1}{1 + \left(\frac{\hat{\Sigma}_{hH}}{M_h^2 - m_H^2 + \hat{\Sigma}_H}\right)^2} \\ &= \frac{1}{1 + \tan^2\Delta\alpha} = \cos^2\Delta\alpha . \end{aligned} \tag{22}$$

Analogously one obtains

$$Z_H = \cos^2\Delta\alpha . \tag{23}$$

At the tree level, the vertex functions can be written as

$$\left.\begin{aligned} \Gamma_h &= \tfrac{ie m_f \sin\alpha}{2 s_W M_W \cos\beta} = C_f^{(d)} \sin\alpha \\ \Gamma_H &= \tfrac{-ie m_f \cos\alpha}{2 s_W M_W \cos\beta} = -C_f^{(d)} \cos\alpha \end{aligned}\right\} \text{for d-type fermions} \tag{24}$$

$$\left.\begin{aligned} \Gamma_h &= \tfrac{-ie m_f \cos\alpha}{2 s_W M_W \sin\beta} = C_f^{(u)} \cos\alpha , \\ \Gamma_H &= \tfrac{-ie m_f \sin\alpha}{2 s_W M_W \sin\beta} = C_f^{(u)} \sin\alpha \end{aligned}\right\} \text{for u-type fermions} . \tag{25}$$

Incorporating them into the decay amplitude yields:

$$\begin{aligned} A_{\rm eff}(h \to f\bar{f}) &= \sqrt{Z_h}\,(\Gamma_h + Z_{hH}\,\Gamma_H) \\ &= C_f^{(d)} \cos\Delta\alpha\,(\sin\alpha - \tan\Delta\alpha\,(-\cos\alpha)) \\ &= C_f^{(d)} \sin(\alpha + \Delta\alpha) \\ &\equiv C_f^{(d)} \sin\alpha_{\rm eff} \text{ (for d-type fermions)} \end{aligned} \tag{26}$$

$$A_{\rm eff}(h \to f\bar{f}) \equiv C_f^{(u)} \cos\alpha_{\rm eff} \text{ (for u-type fermions)} \tag{27}$$

$$A_{\rm eff}(H \to f\bar{f}) \equiv -C_f^{(d)} \cos\alpha_{\rm eff} \text{ (for d-type fermions)} \tag{28}$$

$$A_{\rm eff}(H \to f\bar{f}) \equiv C_f^{(u)} \sin\alpha_{\rm eff} \text{ (for u-type fermions)} \tag{29}$$

Recalling the relations

$$D(\alpha_{\rm eff}) = D(\alpha)\, D(\Delta\alpha) \tag{30}$$

and

$$\begin{pmatrix} \hat{\Sigma}_H & \hat{\Sigma}_{hH} \\ \hat{\Sigma}_{hH} & \hat{\Sigma}_h \end{pmatrix} = D^{-1}(\alpha) \begin{pmatrix} \hat{\Sigma}_{\phi_1} & \hat{\Sigma}_{\phi_1\phi_2} \\ \hat{\Sigma}_{\phi_1\phi_2} & \hat{\Sigma}_{\phi_2} \end{pmatrix} D(\alpha) \tag{31}$$

it is obvious that $\alpha_{\rm eff} = (\alpha + \Delta\alpha)$ is exactly the angle that diagonalizes the higher order corrected Higgs boson mass matrix in the ϕ_1, ϕ_2-basis:

$$\begin{array}{c} \begin{pmatrix} m_{\phi_1}^2 - \hat{\Sigma}_{\phi_1} & m_{\phi_1\phi_2}^2 - \hat{\Sigma}_{\phi_1\phi_2} \\ m_{\phi_1\phi_2}^2 - \hat{\Sigma}_{\phi_1\phi_2} & m_{\phi_2}^2 - \hat{\Sigma}_{\phi_2} \end{pmatrix} \xrightarrow{\alpha_{\rm eff}} \begin{pmatrix} M_H^2 & 0 \\ 0 & M_h^2 \end{pmatrix} \\ \downarrow \ \alpha \\ \begin{pmatrix} m_H^2 - \hat{\Sigma}_H & -\hat{\Sigma}_{hH} \\ -\hat{\Sigma}_{hH} & m_h^2 - \hat{\Sigma}_h \end{pmatrix} \xrightarrow{\Delta\alpha} \begin{pmatrix} M_H^2 & 0 \\ 0 & M_h^2 \end{pmatrix} . \end{array} \tag{32}$$

$\alpha_{\rm eff}$ can be obtained from

$$\begin{aligned} \alpha_{\rm eff} &= \arctan\left[\frac{-(M_A^2 + M_Z^2)\sin\beta\,\cos\beta - \hat{\Sigma}_{\phi_1\phi_2}}{M_Z^2\cos^2\beta + M_A^2\sin^2\beta - \hat{\Sigma}_{\phi_1} - M_h^2}\right] , \\ &-\frac{\pi}{2} < \alpha_{\rm eff} < \frac{\pi}{2} . \end{aligned} \tag{33}$$

2.2 The Higgs-boson propagator corrections

For the Higgs boson self-energies employed in (7)–(13) we use the currently most accurate result based on Feynman-diagrammatic calculations. It contains the result of the complete one-loop on-shell calculation of [4], together with the dominant two-loop corrections of $\mathcal{O}(\alpha\alpha_s)$ obtained in [10, 11], including also the leading terms of $\mathcal{O}(G_F^2 m_t^6 / M_W^2)$ [5–7]; the Fortran program *FeynHiggs*, based on this result, has been described in [21]. In this way the complete MSSM one-loop on-shell result together with the dominant two-loop contribution, originating from the $t - \tilde{t}$-sector (without any restrictions on the mixing), is taken into account in the propagator corrections.

In the approach in [10,11] the Higgs boson self-energies are given by:

$$\hat{\Sigma}_s(q^2) = \hat{\Sigma}_s^{(1)}(q^2) + \hat{\Sigma}_s^{(2)}(0) , \quad s = h, H, hH , \tag{34}$$

where the momentum dependence has been neglected only at the two-loop level, while the full momentum dependence is kept in the one-loop contributions.

In a first step of approximation for the calculation of the decay width $\Gamma(h \to f\bar{f})$ the momentum dependence is neglected everywhere in the Higgs boson self-energies (see (14)):

$$\hat{\Sigma}_s(q^2) \to \hat{\Sigma}_s^{(1)}(0) + \hat{\Sigma}_s^{(2)}(0) \ , \quad s = h, H, hH \ . \tag{35}$$

This corresponds to the $\alpha_{\rm eff}$-approximation, as described in Sect. 2.1.

In a second step of approximation we approximate the Higgs boson self-energies by the compact analytical formulas given in [22]:

$$\hat{\Sigma}_s(q^2) = \hat{\Sigma}_s^{(1)\,\rm approx}(0) + \hat{\Sigma}_s^{(2)\,\rm approx}(0) \ , \quad s = h, H, hH, \tag{36}$$

yielding relatively short expressions which allow a very fast numerical evaluation. In the following, this approximation is labeled by $\alpha_{\rm eff}$(approx).

For the $\tilde{t}$-sector, we use the same conventions as in [11]: the scalar top masses and the mixing angle are related to the parameters $M_{\tilde{t}_L}$, $M_{\tilde{t}_R}$ and X_t of the $\tilde{t}$-mass matrix

$$\mathcal{M}^2_{\tilde{t}} = \begin{pmatrix} M^2_{\tilde{t}_L} + m_t^2 + \cos 2\beta \ (\frac{1}{2} - \frac{2}{3} s_W^2) M_Z^2 & m_t X_t \\ m_t X_t & M^2_{\tilde{t}_R} + m_t^2 + \frac{2}{3} \cos 2\beta \ s_W^2 M_Z^2 \end{pmatrix}, \tag{37}$$

with

$$X_t = A_t - \mu \cot\beta \ . \tag{38}$$

In the numerical analysis below we have chosen $m_{\tilde{q}} \equiv M_{\tilde{t}_L} = M_{\tilde{t}_R}$.

In [11, 22] it has been shown that for a given set of MSSM parameters the maximal values of M_h as a function of X_t are obtained for $|X_t/m_{\tilde{q}}| \approx 2$. This case we refer to as 'maximal mixing'. Minimal values for M_h are reached for $X_t \approx 0$. This case we refer to as 'no mixing'.

2.3 Decay width of the lightest Higgs boson

At the tree level, the decay width for $h \to f\bar{f}$ is given by

$$\Gamma_0(h \to f\bar{f}) = N_C \frac{m_h}{8\pi} \left(1 - \frac{4 m_f^2}{m_h^2}\right)^{\frac{3}{2}} |\Gamma_h|^2 \ . \tag{39}$$

The electroweak propagator corrections are incorporated by using the higher-order decay amplitude (8)

$$\Gamma_1 \equiv \Gamma_1(h \to f\bar{f}) = N_C \frac{M_h}{8\pi} \left(1 - \frac{4 m_f^2}{M_h^2}\right)^{\frac{3}{2}} |A(h \to f\bar{f})|^2. \tag{40}$$

The $\alpha_{\rm eff}$-approximation is given by

$$\Gamma_{1,\rm eff} \equiv \Gamma_{1,\rm eff}(h \to f\bar{f}) = N_C \frac{M_h}{8\pi} \left(1 - \frac{4 m_f^2}{M_h^2}\right)^{\frac{3}{2}} \times |A_{\rm eff}(h \to f\bar{f})|^2 \ . \tag{41}$$

In this paper we consider only those electroweak higher-order contributions which enter via the Higgs boson self-energies. These corrections contain the Yukawa contributions of $\mathcal{O}(G_F m_t^4/M_W^2)$, which are the dominant electroweak one-loop corrections to the Higgs-boson decay width, and the corresponding dominant two-loop corrections, see Sect. 2.2. The pure weak $\mathcal{O}(\alpha)$ vertex corrections are neglected (they have been calculated in [12] and were found to be at the level of only a few % for most parts of the MSSM parameter space, see also Sect. 2.3.3 below.)

2.3.1 QED corrections

Here we follow the results given in [12–15]. The IR-divergent virtual photon contribution is taken into account in combination with real-photon bremsstrahlung yielding the QED corrections. The contribution to the decay width induced by γ-exchange and final-state photon radiation can be cast into the very compact formula

$$\Delta\Gamma_\gamma = \Gamma_1 \cdot \delta\Gamma_\gamma \ , \tag{42}$$

where for $m_f^2 \ll M_h^2$ the factor $\delta\Gamma_\gamma$ has the simple form

$$\delta\Gamma_\gamma = \frac{\alpha}{\pi} Q_f^2 \left[-3 \log\left(\frac{M_h}{m_f}\right) + \frac{9}{4}\right] \ . \tag{43}$$

2.3.2 QCD corrections: gluon contributions

The corresponding results have been obtained in [12–18]. The additional contribution to the decay width induced by gluon exchange and final-state gluon radiation can be incorporated into (40) by writing

$$\Gamma_{1,g} = \Gamma_1 \cdot \frac{m_q^2(M_h^2)}{m_q^2} \left[1 + \frac{\alpha_s(M_h^2)}{\pi} \times \left\{ C_F \frac{9}{4} + \frac{8}{3} \left(1 - \frac{\alpha_s(m_b^2)}{\alpha_s(M_h^2)}\right) \right\} \right] \ . \tag{44}$$

The correction factor containing $\alpha_s(m_b^2)$, which has not been included in previous diagrammatic calculations, can give rise to non-negligible contributions. $m_q(M_h^2)$ is calculated via

$$m_q(q^2) = m_q \frac{c(q^2)}{c(m_q^2)} \ , \tag{45}$$

$$c(q^2) = \left(\frac{\beta_0 \alpha_s(q^2)}{2\pi}\right)^{-\gamma_0/2\beta_0} \left[1 + \frac{(\beta_1\gamma_0 - \beta_0\gamma_1)}{\beta_0^2} \frac{\alpha_s(q^2)}{8\pi} + \left(\frac{(\beta_1\gamma_0 - \beta_0\gamma_1)^2}{2\beta_0^4} + \frac{\gamma_0(\beta_2\beta_0 - \beta_1^2)}{\beta_0^3} + \frac{\gamma_1\beta_1}{\beta_0^2} - \frac{\gamma_2}{\beta_0} \right) \left(\frac{\alpha_s(q^2)}{8\pi}\right)^2 \right] , \tag{46}$$

where m_q is the pole mass and $m_q(m_q^2) = m_q$. The coefficients in (46) are:

$$\begin{aligned}
\beta_0 &= \frac{33-2N_f}{3} \ , \\
\beta_1 &= 102 - \frac{38}{3}N_f \ , \\
\beta_2 &= \frac{2857}{2} - \frac{5033}{18}N_f + \frac{325}{54}N_f^2 \ , \\
\gamma_0 &= -8 \ , \\
\gamma_1 &= -\frac{404}{3} + \frac{40}{9}N_f \ , \\
\gamma_2 &= \frac{2}{3}\left[\frac{140}{27}N_f^2 + \left(160\zeta(3) + \frac{2216}{9}\right)N_f - 3747\right], \qquad (47)
\end{aligned}$$

where $\zeta(3) \approx 1.2020596\ldots$ and $N_f = 5$ for $f = c, b$, which are considered here. The strong coupling constant α_s is given up to three loops by:

$$\begin{aligned}
\alpha_s(q^2) = \frac{4\,\pi}{\beta_0 L_q}\Bigg[1 - \frac{\beta_1}{\beta_0^2}\frac{\log L_q}{L_q} + \frac{\beta_1^2}{\beta_0^4}\frac{\log^2 L_q}{L_q^2} \\
- \frac{\beta_1^2}{\beta_0^4}\frac{\log L_q}{L_q^2} + \frac{\beta_2\beta_0 - \beta_1^2}{\beta_0^4}\frac{1}{L_q^2}\Bigg] \ , \qquad (48)
\end{aligned}$$

where $L_q = \log(q^2/\Lambda^2_{\rm QCD})$. (For the numerical evaluation $\Lambda_{\rm QCD} = 220$ MeV has been used.) Numerically, more than 80% of the gluon-exchange contribution is absorbed into the running quark mass.

2.3.3 QCD corrections: gluino contributions

We follow the calculation given in [12][1], similar results can also be found in [17]. The additional contributions to the decay width induced by gluino-exchange are incorporated via

$$\Delta\Gamma_{\tilde g} = \Gamma_1 \cdot \delta\Gamma_{\tilde g} \ , \qquad (49)$$

where $\delta\Gamma_{\tilde g}$ is given by

$$\delta\Gamma_{\tilde g} = \frac{2}{\Gamma_h + Z_{hH}\Gamma_H}{\rm Re}\left[\Gamma^h_{\tilde g} + Z_{hH}\Gamma^H_{\tilde g}\right] \qquad (50)$$

for real Z_{hH} (i.e. neglecting the imaginary part in (50)); $\Gamma^h_{\tilde g}$ and $\Gamma^H_{\tilde g}$ are given by

$$\begin{aligned}
\Gamma^h_{\tilde g} = \Gamma_h \Bigg[\Delta T^h_{\tilde g}\Big|_{q^2=M_h^2} + \Sigma^f_{S,\tilde g}(m_q^2) \\
-2m_q^2\left(\Sigma^{f\prime}_{S,\tilde g}(m_q^2) + \Sigma^{f\prime}_{V,\tilde g}(m_q^2)\right)\Bigg] \qquad (51)
\end{aligned}$$

$$\begin{aligned}
\Gamma^H_{\tilde g} = \Gamma_H \Bigg[\Delta T^H_{\tilde g}\Big|_{q^2=M_h^2} + \Sigma^f_{S,\tilde g}(m_q^2) \\
-2m_q^2\left(\Sigma^{f\prime}_{S,\tilde g}(m_q^2) + \Sigma^{f\prime}_{V,\tilde g}(m_q^2)\right)\Bigg]. \qquad (52)
\end{aligned}$$

[1] An error in [12] concerning the proper inclusion of the $Hf\bar f$ coupling has been corrected.

$\Delta T^{h,H}_{\tilde g}$ denote the gluino vertex-corrections, whereas Σ^f represents the gluino contribution to the fermion self-energy corrections. Explicit expressions for these terms can be found in [12].

For large values of $\tan\beta$ in combination with large values of $|\mu|$, the gluino-exchange corrections to $\Gamma(h \to b\bar b)$ can become very large. In [23, 24] as well as in [25] it has been proposed to derive an effective contribution to the decay width resummed to all orders. A similar resummation can be applied for weak $\mathcal{O}(\alpha)$ chargino-exchange corrections to $\Gamma(h \to b\bar b)$, where they become non-negligible [23]. In the numerical examples given in [25] the difference between the one-loop result for $\Gamma(h \to f\bar f)$ and the effectively resummed result does not exceed 10 – 15%, even for very large values of $\tan\beta > 40$. A proof of how the resummation of the leading terms arising for large $\tan\beta$ can be performed for the $H^+\bar t b$ vertex is given in [26]. Concerning our numerical analysis in Sect. 3 we have neglected the additional contributions from the resummation. These additional corrections, although potentally large in some regions of the MSSM parameter space, would not qualitatively change our conclusions given below. A more detailed investigation of the effects of a proper resummation of the leading contributions and of the inclusion of the complete electroweak one-loop vertex corrections will be given in a forthcoming publication.

For some parameter combinations the gluino corrections can drive $\Gamma(h \to b\bar b)$ to very small values, see the discussion at the end of Sect. 3.1.

2.3.4 Decay width and branching ratio

Including the various types of corrections, the decay width is given by

$$\Gamma(h \to f\bar f) = \Gamma_{1,g} + \Delta\Gamma_\gamma + \Delta\Gamma_{\tilde g} \ . \qquad (53)$$

Summing over $f = b, c, \tau$ and adding $\Gamma(h \to gg)$ (which can be numerically relevant [27]), results in an approximation for the total decay width

$$\Gamma_{\rm tot} = \sum_{f=b,c,\tau}\Gamma(h \to f\bar f) + \Gamma(h \to gg) \ . \qquad (54)$$

We do not take into account the decay $h \to AA$ (see e.g. [28] for a detailed study). Although it is dominant whenever it is kinematically allowed, it plays a role only for very small values of $\tan\beta$ ($\tan\beta \lesssim 1.5$) which will not be considered here because of the limits obtained at LEP2 [29]. We also assume that all other SUSY particles are too heavy to allow further decay channels. In addition, we neglect the decay $h \to WW^*$ which can be of $\mathcal{O}(1\%)$ for $M_h \gtrsim 100$ GeV.

The fermionic branching ratio is defined by

$$R_f \equiv BR(h \to f\bar f) = \frac{\Gamma(h \to f\bar f)}{\Gamma_{\rm tot}} \ . \qquad (55)$$

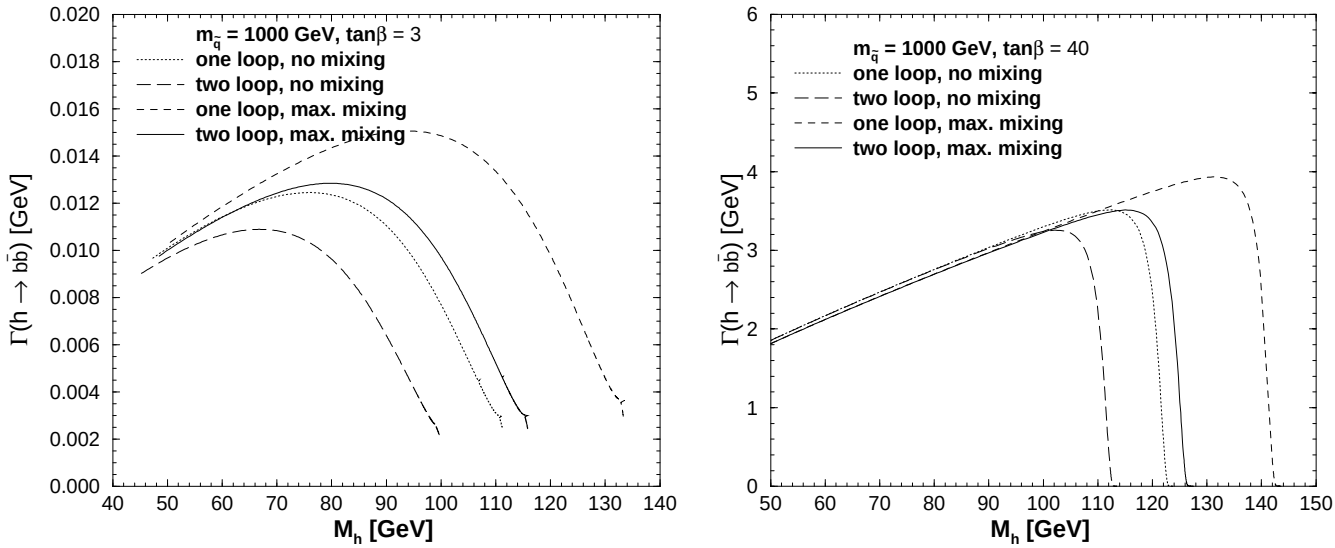

Fig. 1. $\Gamma(h \to b\bar{b})$ is shown as a function of M_h. The Higgs-propagator corrections have been evaluated at the one- and at the two-loop level. The QED, gluon and gluino contributions are included. The other parameters are $\mu = -100$ GeV, $M_2 = m_{\tilde{q}}$, $m_{\tilde{g}} = 500$ GeV, $A_b = A_t$, $\tan\beta = 3, 40$. The result is given in the no-mixing and maximal-mixing scenario

3 Numerical analysis

Concerning the numerical evaluation of the Higgs-boson propagator corrections, we follow Sect. 2.2. For $\tan\beta$ we have chosen two representative values, a relatively low value, $\tan\beta = 3$,[2] and a high value, $\tan\beta = 40$. For sake of comparison we also consider an intermediate value of $\tan\beta = 20$ in some cases. If not indicated differently, the other MSSM parameters are chosen as follows: $\mu = -100$ GeV, $M_2 = m_{\tilde{q}}$ (M_2 is the soft SUSY-breaking term in the gaugino sector), gluino mass $m_{\tilde{g}} = 500$ GeV, $A_b = A_t$ (which fixes, together with μ, the mixing in the $\tilde{b}$-sector). For the SM fermion masses we have furthermore chosen $m_t = 175$ GeV, $m_b = 4.5$ GeV[3] , $m_\tau = 1.777$ GeV and $m_c = 1.5$ GeV.

The mass M_A of the $\mathcal{CP}$-odd Higgs boson is treated as an input parameter and is varied in the interval 50 GeV $\leq M_A \leq 500$ GeV. The corresponding values for M_h follow from (7). M_h, derived in this way, subsequently enters the numerical evaluation of the formulas presented in Sect. 2. Thus the variation of M_h in the plots stems from the variation of M_A in the above given range.

[2] This values is well above the expected limit obtainable at the end of LEP, assuming that no Higgs boson signal will be found [29]. For these expected limits $m_t = 174.3$ GeV and $m_{\tilde{q}} = 1$ TeV has been assumed.

[3] The value of $m_h = 4.5$ GeV is used in the tree-level expression and in the QED and QCD vertex corrections (see Sects. 2.3.1 - 2.3.3), while for the Higgs-propagator corrections the running bottom mass, $m_b(m_t) = 2.97$ GeV, has been used, in order to partially absorb higher-order QCD corrections.

3.1 Effects of the two-loop Higgs-propagator corrections

We first focus on the effects of the two-loop Higgs-boson propagator corrections. They have been evaluated at the one- and at the two-loop level as described in Sect. 2.2. Fig. 1 shows the results for $\Gamma(h \to b\bar{b})$ for a common scalar quark mass $m_{\tilde{q}} = 1000$ GeV and $\tan\beta = 3$ and $\tan\beta = 40$ in the no-mixing and the maximal-mixing scenario. The QED and the QCD gluon and gluino vertex contributions are also included.

In the small $\tan\beta$ scenario, larger values for $\Gamma(h \to b\bar{b})$ are obtained for maximal mixing. The two-loop corrections strongly reduce the decay width. In the large $\tan\beta$ scenario the variation is mainly a kinematical effect from the different values of M_h at the one- and two-loop level. The absolute values obtained for $\Gamma(h \to b\bar{b})$ are three orders of magnitude higher in the $\tan\beta = 40$ scenario, which is due to the fact that $\Gamma(h \to b\bar{b}) \sim 1/\cos^2\beta$.

In Fig. 2 the three decay rates $\Gamma(h \to b\bar{b})$, $\Gamma(h \to \tau^+\tau^-)$ and $\Gamma(h \to c\bar{c})$ are shown as a function of M_h. The results are given in the no-mixing scenario for $m_{\tilde{q}} = 500$ GeV and $\tan\beta = 3, 40$.

In the low $\tan\beta$ scenario $\Gamma(h \to b\bar{b})$ and $\Gamma(h \to \tau^+\tau^-)$ are lowered at the two-loop level, while $\Gamma(h \to c\bar{c})$ is increased. The decay rate for $h \to b\bar{b}$ is about one and two orders of magnitude larger compared to the ones of $h \to \tau^+\tau^-$ and $h \to c\bar{c}$, respectively. In the large $\tan\beta$ scenario the shifts are again dominated by the kinematical effect from the different values of M_h at the one- and two-loop level. In the maximal-mixing case, which is not plotted here, we find qualitatively the same behavior.

We now turn to the effects of the two-loop corrections to the branching ratios. For not too large values of M_h, $\Gamma_{\rm tot}$ is strongly dominated by $\Gamma(h \to b\bar{b})$. For large values of M_h the decay into gluons becomes more relevant.

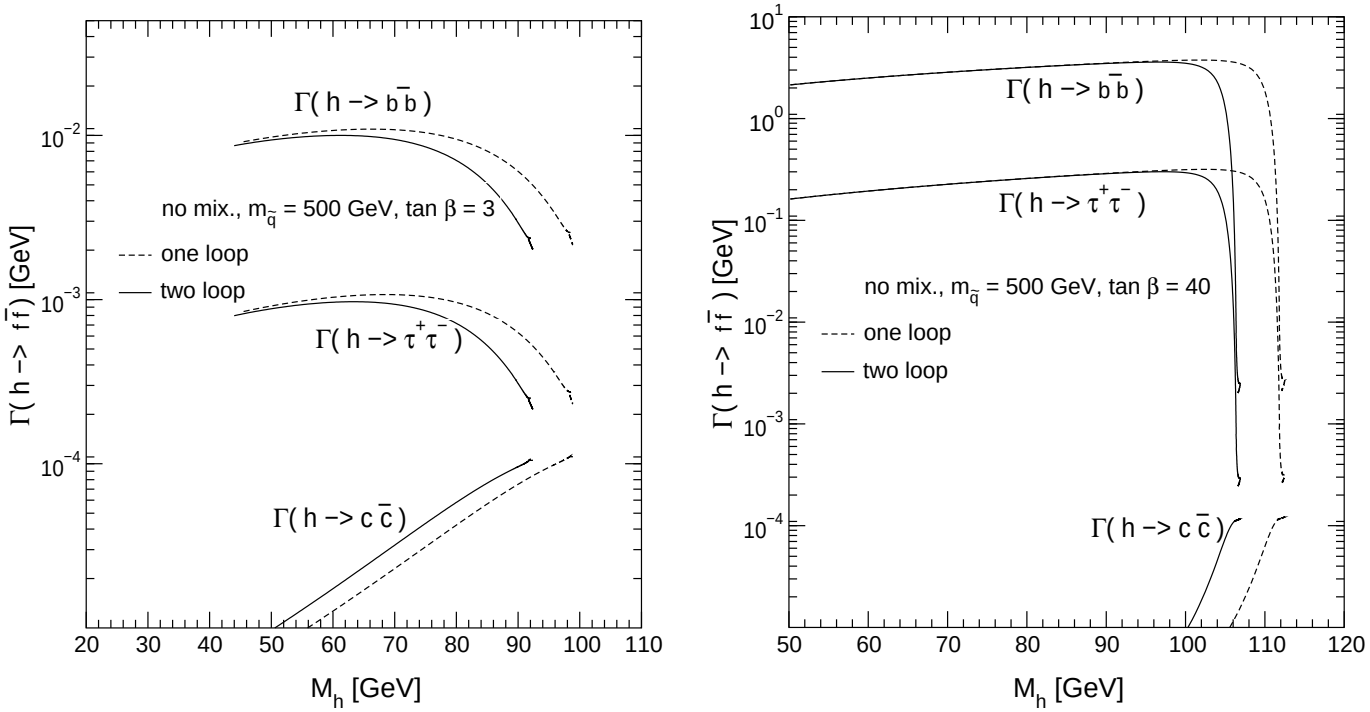

Fig. 2. $\Gamma(h \to b\bar{b})$, $\Gamma(h \to \tau^+\tau^-)$ and $\Gamma(h \to c\bar{c})$ are shown as a function of M_h. The Higgs-propagator corrections have been evaluated at the one- and at the two-loop level. The QED, gluon and gluino contributions are included. The other parameters are $\mu = -100$ GeV, $M_2 = m_{\tilde{q}}$, $m_{\tilde{g}} = 500$ GeV, $A_b = A_t$, $\tan\beta = 3, 40$. The result is given in the no-mixing scenario

In Fig. 3 we show the branching ratio $BR(h \to b\bar{b})$ as a function of M_h and M_A. For values of $M_A \gtrsim 250$ GeV there is a non-negligible difference between one-loop and two-loop order, where at the two-loop level the branching ratio is slightly enhanced. Compared in terms of M_h there is nearly no change for small values of M_h in the low and in the high $\tan\beta$ case. Here $BR(h \to b\bar{b})$ is changed by less than about 1%, see Fig. 3. $BR(h \to \tau^+\tau^-)$ is increased by less than about 2%. $BR(h \to c\bar{c})$ can be increased at the two-loop level by $\mathcal{O}(50\%)$, but remains numerically relatively small. For $\tan\beta = 40$ the main difference arises at the endpoints of the spectrum, again due to the fact that different Higgs boson masses can be obtained at the one-loop and at the two-loop level. For $\tan\beta = 3$, however, also several GeV below the kinematical endpoints there is a sizable effect on $BR(h \to b\bar{b})$. Thus, in the experimentally allowed region of M_h, the two-loop corrections can have an important effect on $BR(h \to b\bar{b})$.

Higgs boson search, especially at e^+e^- colliders, often relies on b search, since on one hand the lightest $\mathcal{CP}$-even Higgs boson decays dominantly into $b\bar{b}$ and on the other hand b tagging can be performed with high efficiency. For some combinations of parameters, however, $\Gamma(h \to b\bar{b})$ can become very small and thus $BR(h \to b\bar{b})$ can approach zero as a consequence of large Higgs-boson propagator corrections or large gluino vertex-corrections, making Higgs boson search possibly very difficult for these parameters. Within the effective potential approach this kind of effect has first been observed in [30], recent analyses investigating the parameter regions where $BR(h \to b\bar{b})$ is suppressed can be found in [23, 24]. In order to have reliable predictions for these regions of parameter space a full calculation of the one-loop vertex corrections, including all $\mathcal{O}(\alpha)$ contributions, would be necessary. Here we demonstrate the effect of the two-loop propagator corrections on the values of the parameters, especially of M_A, for which $BR(h \to b\bar{b})$ goes to zero. We also show the impact of the inclusion of the momentum dependence of the Higgs boson self-energies (see (7) and (14)), that is often neglected in phenomenological analyses of the decays of the lightest $\mathcal{CP}$-even Higgs boson.

In Fig. 4 $BR(h \to b\bar{b})$ is shown as a function of M_A. The Higgs boson self-energies are evaluated at the one-loop and at the two-loop level with and without momentum dependence (see (14)). The other parameters are $\tan\beta = 25$, $m_{\tilde{q}} = 500$ GeV, $m_{\tilde{g}} = 400$ GeV, $M_2 = 400$ GeV, $X_t = 400$ GeV, $A_b = A_t$, $\mu = -1000$ GeV. The inclusion of the two-loop propagator corrections shifts the M_A value for which $BR(h \to b\bar{b})$ becomes very small by about -35 GeV. The inclusion of the momentum dependence of the Higgs boson self-energies induces another shift of about -6 GeV. In order to have reliable phenomenological predictions for the problematic M_A values the two-loop corrections as well as the inclusion of the momentum dependence is necessary. Note that the inclusion of the gluino vertex corrections as well as the purely weak vertex corrections can also have a large impact on the critical M_A values.

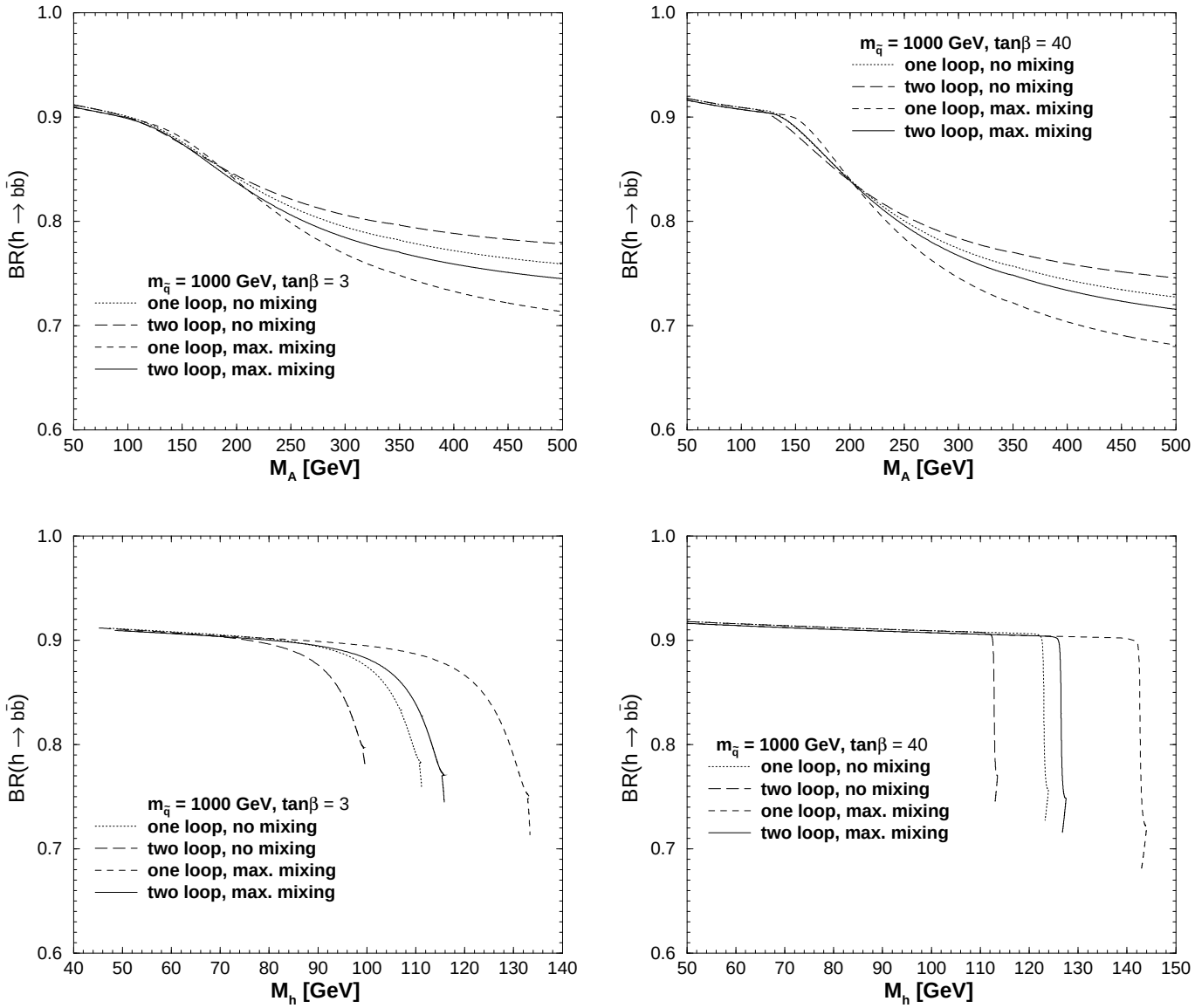

Fig. 3. $BR(h \to b\bar{b})$ is shown as a function of M_A and M_h for the same settings as in Fig. 1. The QED, gluon and gluino contributions are included

3.2 Effects of the gluino vertex corrections

In this subsection we present the effect of the gluino-exchange contribution to the $hf\bar{f}$ vertex corrections. These corrections have been neglected so far in most phenomenological analyses[4].

Figure 5 shows $\Gamma(h \to b\bar{b})$ in three steps of accuracy: the dotted curves contain only the pure self-energy correction, the dashed curves contain in addition the QED and the gluon-exchange correction. The solid curves show the full results, including also the gluino-exchange correction. The results are shown for the no mixing scenario, $\mu = -100$ GeV, $m_{\tilde{g}} = 500$ GeV, $m_{\tilde{q}} = 200, 1000$ GeV in the left and right part of Fig. 5, respectively. For $\tan\beta$, three values have been chosen: $\tan\beta = 3, 20, 40$.

The left plot of Fig. 5 corresponds to a small soft SUSY-breaking scale, $m_{\tilde{q}} = 200$ GeV. The effect of the gluon contribution is large and negative, the effect of the QED correction is small. For this combination of $m_{\tilde{g}}$, $m_{\tilde{q}}$ and μ the effect of the gluino correction is large and positive as can be seen from the transition from the dashed to the solid curves. For $\tan\beta = 40$ it nearly compensates the gluon effect, for $\tan\beta = 20$ it amounts up to 20% of the gluonic correction, while for $\tan\beta = 3$ the gluino-exchange contribution is negligible. Note that we have chosen a relatively small value of μ, $\mu = -100$ GeV. For larger values of $|\mu|$ even larger correction can be obtained. Hence neglecting the gluino-exchange correction in the large $\tan\beta$ scenario can lead to results which deviate by 50% from

[4] The gluino-exchange contributions are currently incorporated into HDECAY [19,31]. Concerning the discovery potential of LEP, the Tevatron and the LHC, the gluino corrections have also been studied recently in [24,25].

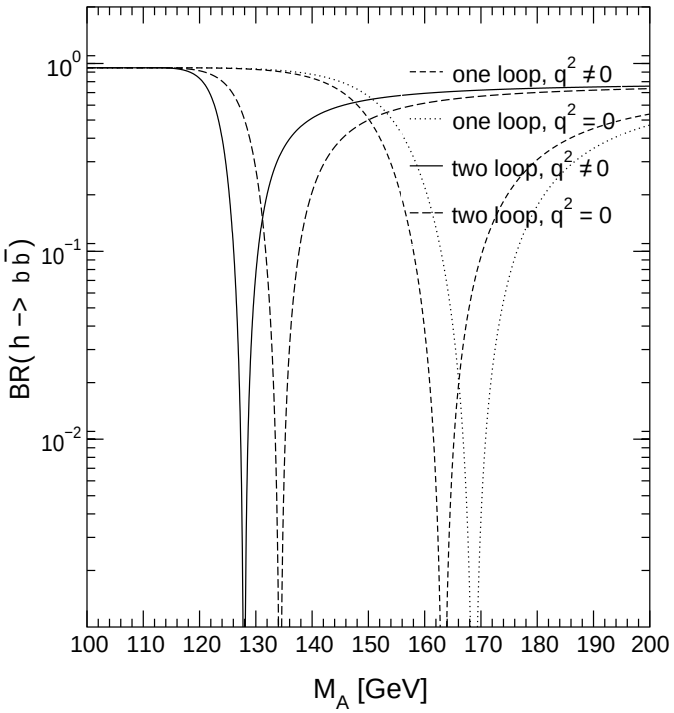

Fig. 4. $BR(h \to b\bar{b})$ is shown as a function of M_A. The Higgs boson self-energies are evaluated at the one-loop and at the two-loop level with and without momentum dependence (see (14)). The other parameters are $\tan\beta = 25$, $m_{\tilde{q}} = 500$ GeV, $m_{\tilde{g}} = 400$ GeV, $M_2 = 400$ GeV, $X_t = 400$ GeV, $A_b = A_t$, $\mu = -1000$ GeV

the full $\mathcal{O}(\alpha_s)$ calculation (see also Sect. 2.3.3). The right plot of Fig. 5 corresponds to $m_{\tilde{q}} = 1000$ GeV. The gluino-exchange effects are still visible, but much smaller than for $m_{\tilde{q}} = 200$ GeV. The same observation has already been made in [12]. In the maximal-mixing scenario we find qualitatively the same behavior for the gluino-exchange corrections as in the no-mixing scenario.

In Fig. 6 the pure gluino-exchange effect is shown as a function of μ. This effect increases with rising[5] $m_{\tilde{g}}$ and $|\mu|$, where for negative (positive) μ there is an enhancement (a decrease) in $\Gamma(h \to b\bar{b})$. The size of the gluino-exchange contribution also depends on M_A, where larger effects correspond to smaller values of M_A, see also [12]. The small difference between the curves where the decay rate has been calculated without gluino contribution is due to the variation of M_h induced by different values of $m_{\tilde{g}}$ which enters at $\mathcal{O}(\alpha\alpha_s)$. Fig. 6 demonstrates again that neglecting the gluino contribution in the fermion decay rates can yield (strongly) misleading results.

The gluino exchange contribution has only a relatively small impact on $BR(h \to b\bar{b})$. It can have a large influence, on the other hand, on $BR(h \to \tau^+\tau^-)$. Both branching ratios are expected to be measurable at the same level of accuracy, see e.g. [32]. While the Higgs-propagator contributions are universal corrections that affect $\Gamma(h \to b\bar{b})$ and $\Gamma(h \to \tau^+\tau^-)$ in the same way (i.e. the influence on the effective coupling is the same in both cases), the gluino corrections, which influence only $\Gamma(h \to b\bar{b})$, can lead to a different behavior of the two decay widths. In Fig. 7 we show $BR(h \to \tau^+\tau^-)$ as a function of $m_{\tilde{g}}$. The left plot corresponds to three different values of $\tan\beta$ and $\mu = \pm 100$ GeV, $M_A = 100$ GeV. Here we have furthermore chosen $m_{\tilde{q}} = 500$ GeV and moderate mixing, i.e. $X_t = m_{\tilde{q}}$; we find similar results for the other mixing scenarios. For positive (negative) μ the decay rate $\Gamma(h \to b\bar{b})$ is reduced (enhanced), see Fig. 6, thus $BR(h \to \tau^+\tau^-)$ is increased (decreased) by up to 50%. For large values of $m_{\tilde{g}}$ and $\tan\beta$, $BR(h \to \tau^+\tau^-)$ can thus be considerably different from the case where the gluino-exchange contribution to $\Gamma(h \to b\bar{b})$ has been neglected. This becomes even more apparent in the right plot of Fig. 7, where the MSSM result, including gluino exchange contribution, is compared to the SM result. Here we also show the scenario with $M_A = 300$ GeV and $\mu = -400$ GeV, where the Higgs sector of the MSSM behaves SM like (i.e. the lightest Higgs boson has almost SM couplings, all other Higgs bosons are heavy). The horizontal lines represent the SM values for the respective Higgs boson masses. The two Higgs boson masses for each line give similar results so that the lines are indistinguishable in the plot. These masses correspond to an averaged value obtained in the MSSM in the interval $0 < m_{\tilde{g}} < 1000$ GeV, where the variation of M_h is about ± 1 GeV (with our choice of $m_{\tilde{q}}$ and X_t). Since the gluino decouples very slowly, there is no decoupling effect for $m_{\tilde{g}} \lesssim 1000$ GeV and the MSSM results can be considerably different from the SM result, for $M_A = 100$ GeV as well as for $M_A = 300$ GeV, i.e. even where the MSSM Higgs sector behaves otherwise SM like. The deviation can amount up to 50% for $M_A = \mathcal{O}(100$ GeV) and up to 30% for $M_A = \mathcal{O}(300$ GeV). Thus the measurement of $BR(h \to \tau^+\tau^-)$ can provide a distinction between the SM and the MSSM even for relatively large M_A and large $m_{\tilde{g}}$ if also $|\mu|$ and $\tan\beta$ are sufficiently large. The branching ratio $BR(h \to b\bar{b})$ on the other hand, changes only by a few per cent for these parameters, so that this change would be much harder to measure.

3.3 The $\alpha_{\rm eff}$-approximation

In this section we investigate the quality of the $\alpha_{\rm eff}$-approximation. In Fig. 8 we display the relative difference between the full result (34) and the $\alpha_{\rm eff}$ result, where the external momentum of the Higgs self-energies has been neglected, see (35). The relative difference $\Delta\Gamma(h \to b\bar{b}) = (\Gamma^{\rm full}(h \to b\bar{b}) - \Gamma^{\alpha_{\rm eff}}(h \to b\bar{b}))/\Gamma^{\rm full}(h \to b\bar{b})$ is shown as a function of M_A for $m_{\tilde{q}} = 1000$ GeV and for three values of $\tan\beta$ in the no mixing and the maximal mixing scenario. Large deviations occur only in the region 100 GeV $\lesssim M_A \lesssim$ 150 GeV, especially for large $\tan\beta$. In this region of parameter space the values of M_h and M_H are very close to each other. This results in a high sensitivity to small deviations in the Higgs boson self-energies

[5] This is correct for all values of $m_{\tilde{g}}$ considered in this work. A maximal effect is reached around $m_{\tilde{g}} \approx 1500$ GeV. The decoupling of the gluino takes place only for very large values, $m_{\tilde{g}} \gtrsim 5000$ GeV.

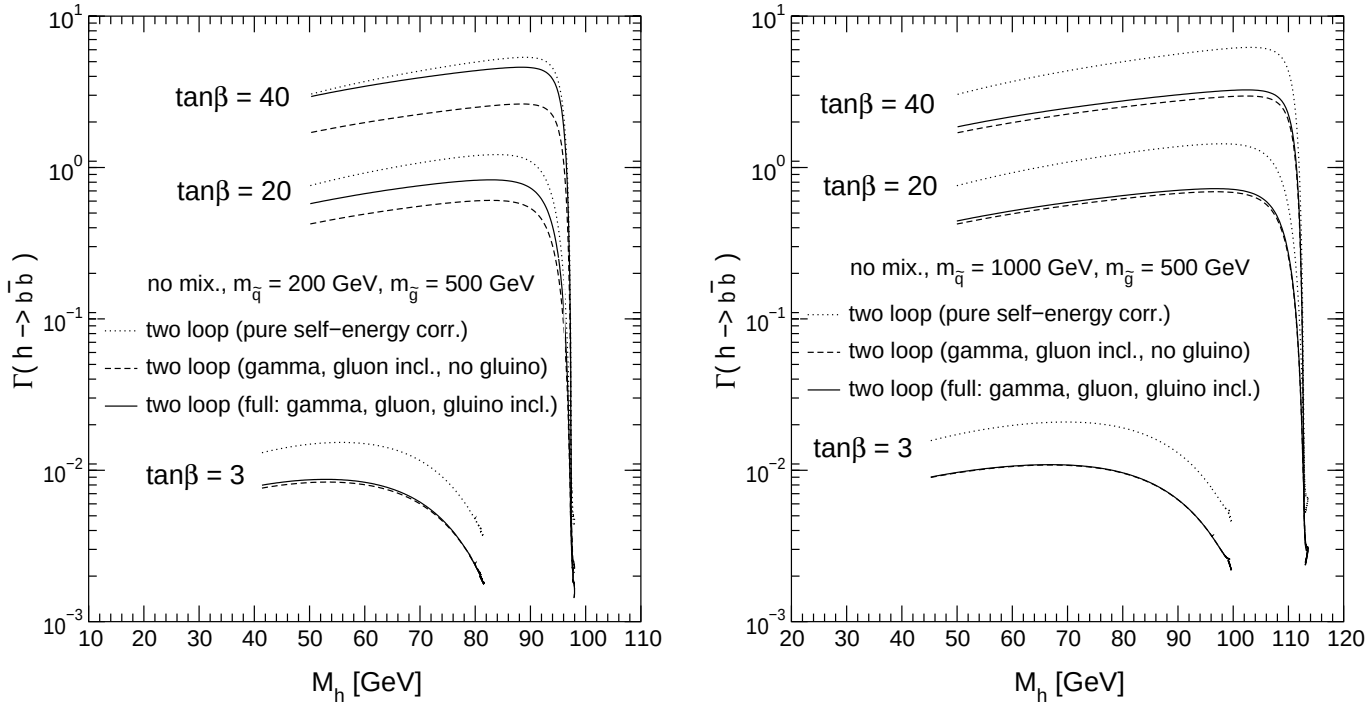

Fig. 5. $\Gamma(h \to b\bar{b})$ is shown as a function of M_h for three values of $\tan\beta$. The Higgs-propagator corrections have been evaluated at the two-loop level in the no-mixing scenario. The dotted curves shows the results containing only the pure self-energy corrections. The results given in the dashed curves in addition contain the QED correction and the gluon-exchange contribution. The solid curves show the full result, including also the gluino correction. The other parameters are $\mu = -100$ GeV, $M_2 = m_{\tilde{q}}$, $A_b = A_t$

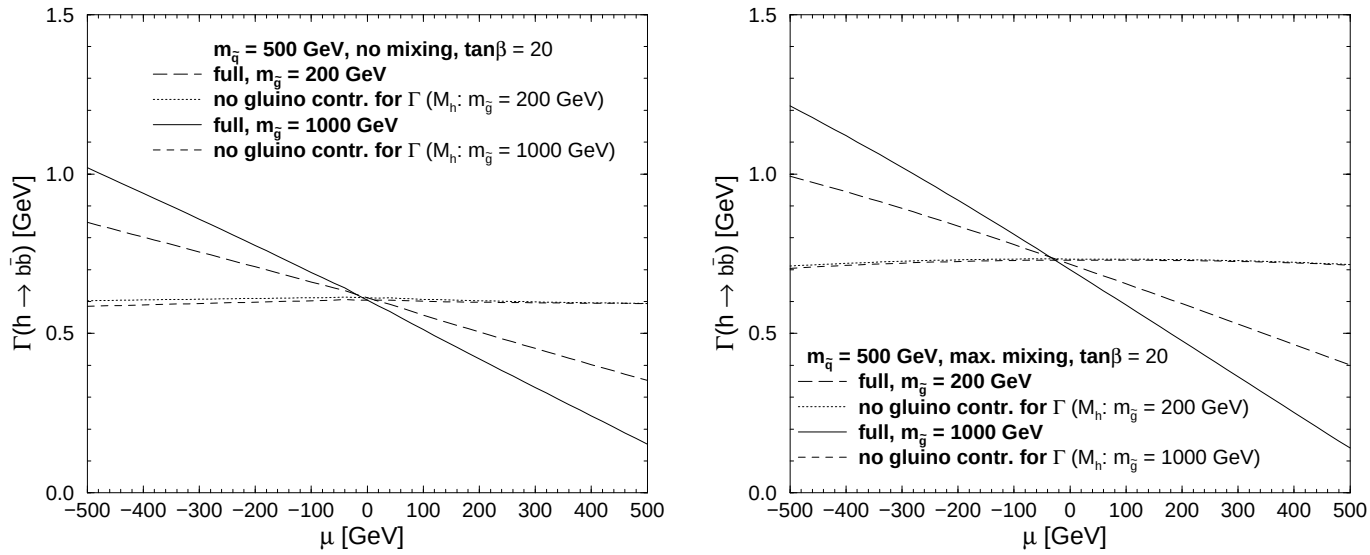

Fig. 6. $\Gamma(h \to b\bar{b})$ is shown as a function of μ for $\tan\beta = 20$ and two different values of $m_{\tilde{g}}$ in the no-mixing and the maximal-mixing scenario. The other parameters are $m_{\tilde{q}} = 500$ GeV, $M_2 = 500$ GeV, $A_b = A_t$, $M_A = 100$ GeV

entering the Higgs-boson mass matrix (7), (15). Another source of differences between the full and the approximate calculation is the threshold $M_A = 2\,m_t = 350$ GeV in the one-loop contribution, originating from the top-loop diagram in the A self-energy and in the AZ self-energy (see [4]). Here the deviation can amount up to 6%.

In Fig. 9 we compare the $\alpha_{\rm eff}$ result (35) with the $\alpha_{\rm eff}$(approx) result (36), where the Higgs boson self-energies have been approximated by the compact analytical expression obtained in [22]. Figure 9 displays the relative difference in the effective mixing angles, $(\sin\alpha_{\rm eff} - \sin\alpha_{\rm eff}({\rm approx}))/\sin\alpha_{\rm eff}$. Via (26) $\sin\alpha_{\rm eff}$ directly determines the decay width $\Gamma(h \to b\bar{b})$. The result is shown for $m_{\tilde{q}} = 1000$ GeV, for three values of $\tan\beta$ in the minimal and the maximal mixing scenario. Apart from the region

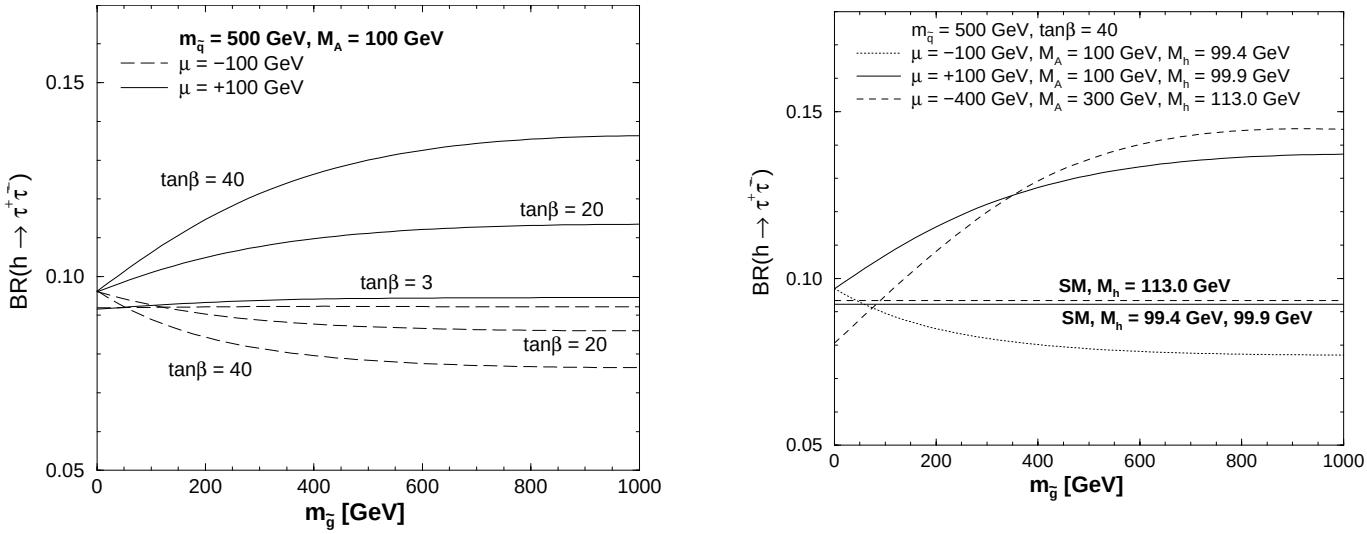

Fig. 7. $BR(h \to \tau^+\tau^-)$ is shown as a function of $m_{\tilde{g}}$. The left plot corresponds to three different values of $\tan\beta$ and $\mu = \pm 100$ GeV. The right plot corresponds to $\tan\beta = 40$ and the two scenarios $M_A = 100$ GeV, $\mu = \pm 100$ GeV and $M_A = 300$ GeV, $\mu = -400$ GeV. The other parameters in both plots are $m_{\tilde{q}} = 500$ GeV, $X_t = 500$ GeV, $M_A = 100$ GeV, $M_2 = 500$ GeV, $A_b = A_t$. The Higgs boson masses given in the legend are averaged masses over the interval $0 < m_{\tilde{g}} < 1000$ GeV where the variation of M_h is about ± 1 GeV for the above considered parameters. The horizontal lines represent the SM result using the corresponding Higgs boson masses

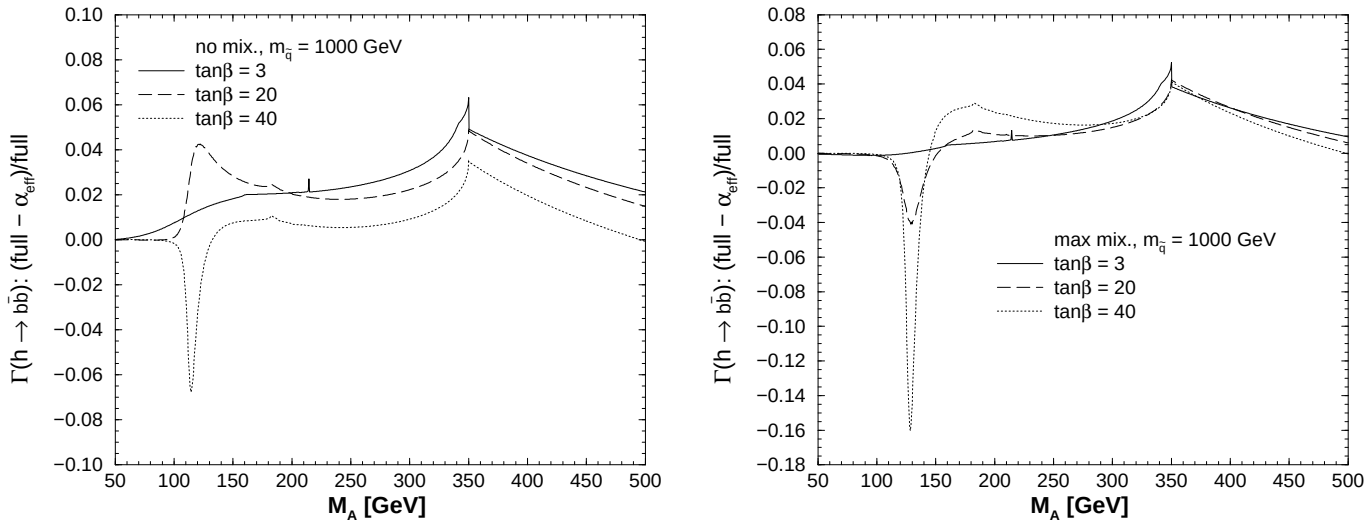

Fig. 8. $\Delta\Gamma(h \to b\bar{b}) = (\Gamma^{\rm full}(h \to b\bar{b}) - \Gamma^{\alpha_{\rm eff}}(h \to b\bar{b}))/\Gamma^{\rm full}(h \to b\bar{b})$ is shown as a function of M_A for three values of $\tan\beta$. The QED, gluon- and gluino-contributions are neglected here. The other parameters are $\mu = -100$ GeV, $M_2 = m_{\tilde{q}}$, $m_{\tilde{g}} = 500$ GeV, $A_b = A_t$, $\tan\beta = 3, 20, 40$. The results are given in the minimal- and the maximal-mixing scenario

around $M_A \approx 120$ GeV (compare Fig. 8) both effective angles agree better than 3% with each other.

Concerning the comparison of the $\alpha_{\rm eff}$-approximations in terms of M_h (which is not plotted here), due to the neglected external momentum or the neglected subdominant one- or two-loop terms, M_h receives a slight shift. Besides this kinematical effect, the decay rate is approximated rather well for most of the M_h values: independently of $m_{\tilde{q}}$, the differences stay mostly below 2-4%, for the no-mixing case as well as for the maximal-mixing case. Only at the endpoints of the spectrum, due to the different Higgs-boson mass values, the difference is not negligible.

4 Comparison with the renormalization group approach

In order to compare our results with those obtained within the renormalization-group-improved effective field theory approach [5, 6] (in the following, for brevity reasons, denoted as RG approach), we made use of the program HDECAY [19]. In Fig. 10 we show the decay rate $\Gamma(h \to b\bar{b})$ as a function of M_h (left part) and as a function of M_A (right part). We compare the RG result of HDECAY, where the gluino-exchange contribution is not yet implemented, with the FD result without and with gluino correction. In order

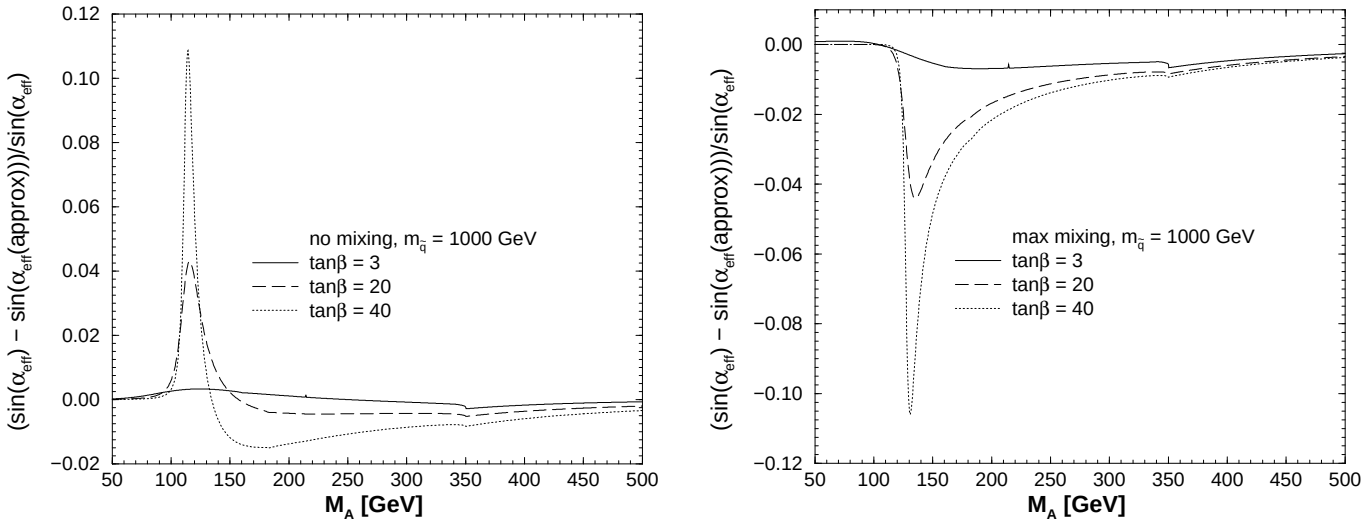

Fig. 9. The relative difference $(\sin\alpha_{\rm eff} - \sin\alpha_{\rm eff}({\rm approx}))/\sin\alpha_{\rm eff}$ (see (35) and (36)) is shown as a function of M_A for three values of $\tan\beta$ in the no mixing and the maximal mixing scenario. The other parameters are chosen as in Fig. 8

to trace back the source of deviations we also show in the lower part of Fig. 10 the sine of the effective mixing angle $\alpha_{\rm eff}$ which enters the decay rate $\Gamma(h \to b\bar{b})$ quadratically (see (26) and (41)). In order to evaluate $\alpha_{\rm eff}$ we have neglected the external momentum (see (35)). As a typical soft SUSY-breaking scale we have chosen $m_{\tilde{q}} = 500$ GeV in Fig. 10. Since the FD and the RG result have been obtained in different renormalization schemes, the entries of the $\tilde{t}$-mass matrix have a different meaning starting from two-loop order [22,33,34]. For the no-mixing case we have set $X_t = 0$ in both approaches, whereas the maximal-mixing case is defined via $X_t = 2\,m_{\tilde{q}}$ for the FD approach and $X_t = \sqrt{6}\,m_{\tilde{q}}$ in the RG approach [22].

In the comparison of the decay rates (and restricting ourselves to the results with neglected gluino exchange), for a given M_h we find deviations for low $\tan\beta$ up to $\mathcal{O}(10\%)$ and agreement better than 4% in the large $\tan\beta$ scenario. The main part of the deviations can be attributed to the deviations in $\alpha_{\rm eff}$ which modify $\Gamma(h \to b\bar{b})$ (see the lower part of Fig. 10). As a general feature, larger deviations arise at the endpoints of the M_h spectrum due to the fact that for the same value of M_A different values for M_h are obtained in the FD and the RG approach, as shown in the left part of Fig. 10. The plots for the $\tan\beta = 40$ scenario show again a sizable effect of the gluino correction.

In Figs. 11 and Fig. 12 the relative differences $\Delta\Gamma(h \to b\bar{b}) = (\Gamma^{\rm FD}(h \to b\bar{b}) - \Gamma^{\rm RG}(h \to b\bar{b}))/\Gamma^{\rm FD}(h \to b\bar{b})$ and $(\sin\alpha_{\rm eff}^{\rm FD} - \sin\alpha_{\rm eff}^{\rm RG})/\sin\alpha_{\rm eff}^{\rm FD}$ are shown as a function of M_A. Comparing $\alpha_{\rm eff}$ as a function of M_A the agreement is relatively good; sizable deviations larger than 10% are found only in the regions where the curves in the right part of Fig. 10 have a steep slope. This can give rise to large deviations up to 50% in $\Gamma(h \to b\bar{b})$ in terms of M_A (for 100 GeV $\lesssim M_A \lesssim$ 150 GeV), as displayed in the right parts of Figs. 11 and 12 (large $\tan\beta$).

5 Conclusions

Using the Feynman-diagrammatic approach for the Higgs-boson propagator corrections, including besides the full one-loop result also the dominant two-loop corrections, we have calculated the decay rates and branching ratios for the decays $h \to b\bar{b}$, $h \to c\bar{c}$ and $h \to \tau^+\tau^-$. We have included the one-loop QED and QCD corrections, where the latter are due to gluon and gluino-exchange contributions. The gluino-exchange corrections have been neglected in most of the previous phenomenological analyses. In the present analysis, only the purely weak $\mathcal{O}(\alpha)$ (process specific) vertex corrections, shown to contribute less than 1% for most parts of the MSSM parameter space, have been neglected.

We have shown analytically that the full set of Higgs-boson propagator corrections for vanishing external momentum can be absorbed into the effective mixing angle, $\alpha_{\rm eff}$, in the neutral $\mathcal{CP}$-even Higgs sector, appearing in the Higgs-boson fermion couplings.

Numerically we have shown that, compared in terms of M_h, the two-loop contributions to the Higgs-boson propagator corrections lead to a sizable decrease for $\Gamma(h \to b\bar{b})$ and $\Gamma(h \to \tau^+\tau^-)$, whereas $\Gamma(h \to c\bar{c})$ can be increased, although it stays relatively small for all sets of parameters we have investigated. A sizable difference in all analyses from the one- to the two-loop calculation arises from the kinematical effect that at the two-loop level lower values for M_h are obtained compared to the one-loop case, thus leading to deviations at the endpoints of the shown M_h spectra. For most parts of the MSSM parameter space the $\alpha_{\rm eff}$-approximation reproduces the full result better than 3%. The gluino-exchange contribution to $\Gamma(h \to b\bar{b})$ has been shown to be sizable for large $\tan\beta$. This correction increases with rising $m_{\tilde{g}}$ and decreases with rising $m_{\tilde{q}}$ and M_A. It is positive (negative) for negative (positive) μ. In the $\tan\beta = 40$ scenario for small $m_{\tilde{q}}$ it nearly compensate the gluon-exchange correction.

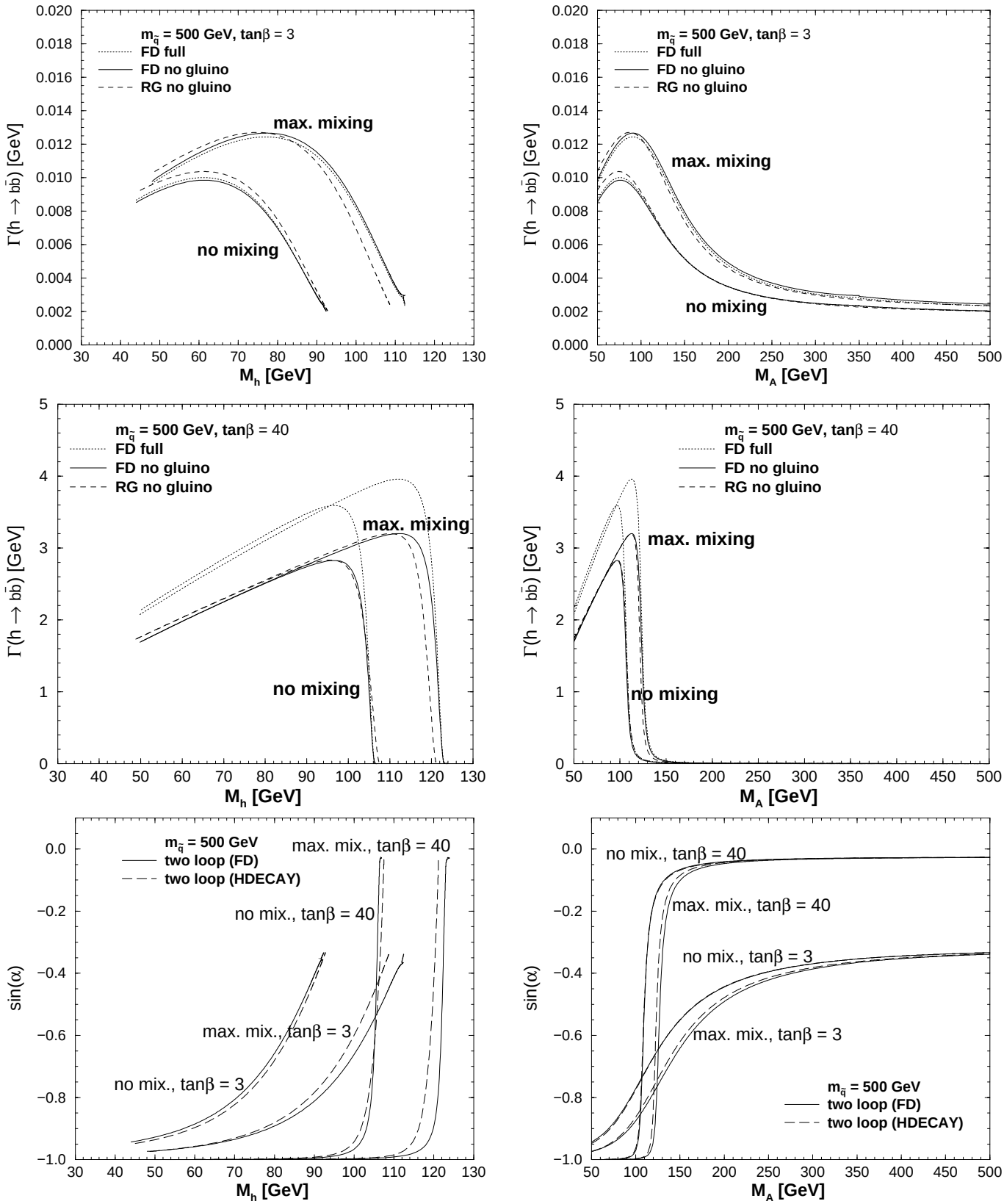

Fig. 10. $\Gamma(h \to b\bar{b})$ is shown as a function of M_h in the left part and as a function of M_A in the right part. The results of the RG approach (without gluino contribution) are compared with the Feynman diagrammatic results (without and with gluino contribution.) The other parameters are $\mu = -100$ GeV, $M_2 = m_{\tilde{q}}$, $m_{\tilde{g}} = 500$ GeV, $A_b = A_t$. In each plot the no-mixing and the maximal-mixing scenarios are shown. In the lower part the sine of the effective mixing angle is shown

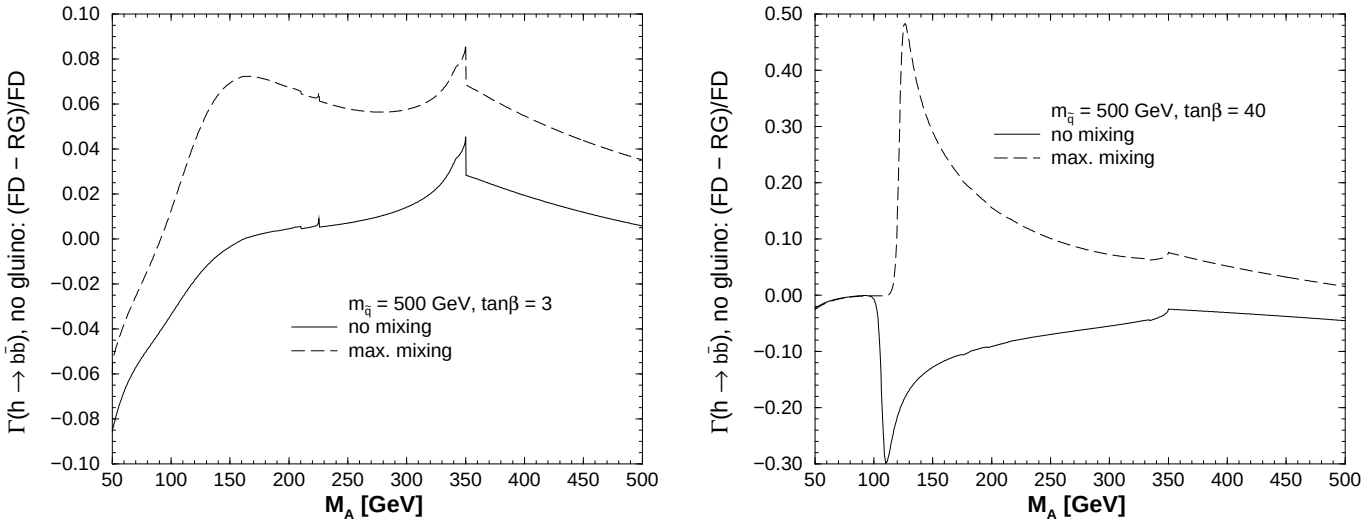

Fig. 11. $\Delta\Gamma(h \to b\bar{b}) = (\Gamma^{\rm FD}(h \to b\bar{b}) - \Gamma^{\rm RG}(h \to b\bar{b}))/\Gamma^{\rm FD}(h \to b\bar{b})$ is shown as a function of M_A for no mixing and maximal mixing. The gluino-contributions are neglected here. The other parameters are $\mu = -100$ GeV, $M_2 = m_{\tilde{q}}$, $m_{\tilde{g}} = 500$ GeV, $A_b = A_t$. The results are given in the low $\tan\beta$ and in the high $\tan\beta$ scenario

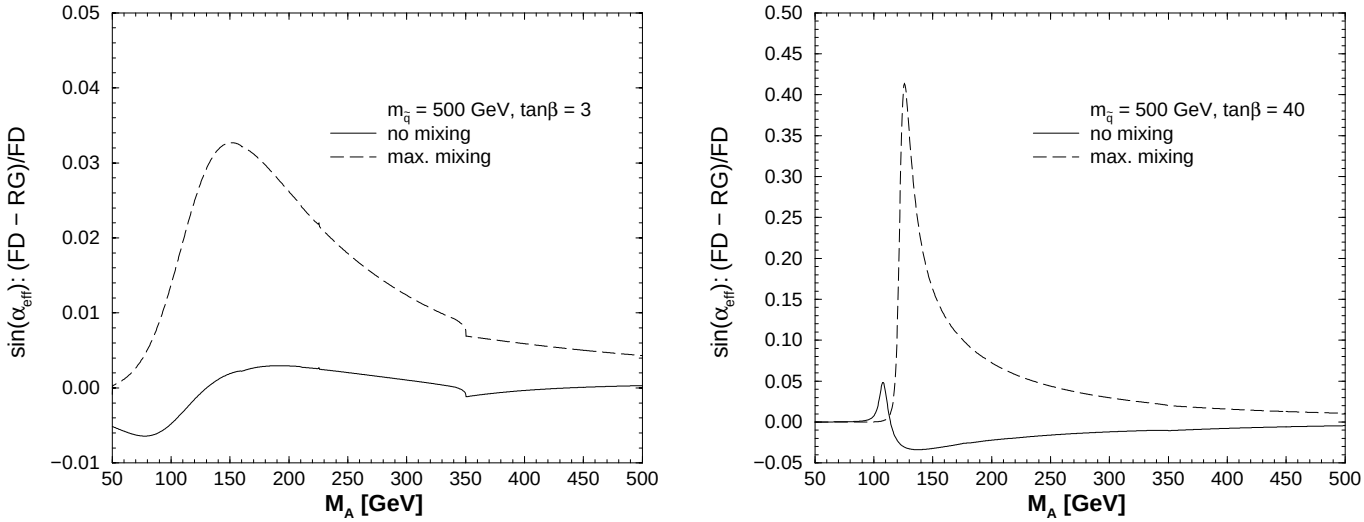

Fig. 12. The relative difference $(\sin\alpha_{\rm eff}^{\rm FD} - \sin\alpha_{\rm eff}^{\rm RG})/\sin\alpha_{\rm eff}^{\rm FD}$ is shown as a function of M_A for two values of $\tan\beta$ in the no mixing and the maximal mixing scenario. The other parameters are chosen as in Fig. 11

The effect of the Higgs-propagator corrections on the branching ratios $BR(h \to f\bar{f})$ is relatively small for small values of M_h, while sizable effects are possible in the experimentally favored region of M_h. The branching ratio $BR(h \to \tau^+\tau^-)$ can receive large corrections up to 50% due to SUSY-QCD corrections to $\Gamma(h \to b\bar{b})$. In some parameter regions the effective $hb\bar{b}$ coupling can become very small, and $BR(h \to b\bar{b})$ can approach zero. In these parameter regions the two-loop contributions as well as the effect of the momentum dependence of the one-loop contributions are particularly important. It should be noted that in order to determine $BR(h \to b\bar{b})$ very precisely in these paremeter regions, also a resummation of the leading terms as well as the inclusion of the complete $\mathcal{O}(\alpha)$ vertex corrections will be necessary.

We have compared our diagrammatic result for $\Gamma(h \to b\bar{b})$ with the result obtained within the renormalization-group-improved effective field theory approach. For the low $\tan\beta$ scenario, compared in terms of M_h, we find deviations up to $\mathcal{O}(10\%)$. In the large $\tan\beta$ scenario the agreement is better than 4%. Compared in terms of M_A, however, differences of up to 50% are possible in the region 100 GeV $\lesssim M_A \lesssim$ 150 GeV. The main part of the deviations can be attributed to the differences in the effective mixing angle $\alpha_{\rm eff}$.

Acknowledgements. We thank M. Spira for valuable discussions and communication about the numerical comparison of our results. We are also grateful to M. Carena, H. Eberl and C. Wagner for interesting and helpful discussions. Parts of the

calculations have been performed on the QCM cluster at the University of Karlsruhe.

References

1. G. Kane, C. Kolda, J. Wells, Phys. Rev. Lett. **70** (1993) 2686, hep-ph/9210242; J. Espinosa, M. Quirós, Phys. Lett. B **302** (1993) 51, hep-ph/9212305; Phys. Rev. Lett. **81** (1998) 516, hep-ph/9804235
2. A. Djouadi, W. Kilian, M. Mühlleitner, P.M. Zerwas, Eur. Phys. Jour. C **10** (1999) 45, DOI 10.1007/s100529900082, hep-ph/9903229
3. H. Haber, R. Hempfling, Phys. Rev. Lett. **66** (1991) 1815; Y. Okada, M. Yamaguchi, T. Yanagida, Prog. Theor. Phys. **85** (1991) 1; J. Ellis, G. Ridolfi, F. Zwirner, Phys. Lett. B **257** (1991) 83; Phys. Lett. B **262** (1991) 477; R. Barbieri, M. Frigeni, Phys. Lett. B **258** (1991) 395
4. A. Dabelstein, Z. Phys. C **67** (1995) 495, hep-ph/9409375
5. M. Carena, J. Espinosa, M. Quirós, C. Wagner, Phys. Lett. B **355** (1995) 209, hep-ph/9504316
6. M. Carena, M. Quirós, C. Wagner, Nucl. Phys. B **461** (1996) 407, hep-ph/9508343
7. H. Haber, R. Hempfling, A. Hoang, Z. Phys. C **75** (1997) 539, hep-ph/9609331
8. R. Hempfling, A. Hoang, Phys. Lett. B **331** (1994) 99, hep-ph/9401219
9. R.-J. Zhang, Phys. Lett. B **447** (1999) 89, hep-ph/9808299
10. S. Heinemeyer, W. Hollik, G. Weiglein, Phys. Rev. D **58** (1998) 091701, hep-ph/9803277; Phys. Lett. B **440** (1998) 296, hep-ph/9807423
11. S. Heinemeyer, W. Hollik, G. Weiglein, Eur. Phys. Jour. C **9** (1999) 343, DOI 10.1007/s100529900006, hep-ph/9812472
12. A. Dabelstein, Nucl. Phys. B **456** (1995) 25, hep-ph/9503443
13. E. Braaten, J.P. Leveille, Phys. Rev. D **22** (1980) 715; N. Sakai, Phys. Rev. D **22** (1980) 2220; T. Inami, T. Kubota, Nucl. Phys. B **179** (1981) 171; A. Dabelstein, W. Hollik, Z. Phys.C **53** (1991) 507
14. D.Y. Bardin, B.M. Vilensky, P.Ch. Christova, Sov. J. Nucl. Phys. **53** (1991) 152
15. M. Drees, K. Hikasa, Phys. Lett. B **240** (1990) 455, E: ibid B **262** (1991) 497
16. P. Chankowski, S. Pokorski, J. Rosiek, Nucl. Phys. B **423** (1994) 497
17. J.A. Coarasa, R.A. Jiménez, J. Solà, Phys. Lett. B **389** (1996) 312, hep-ph/9511402
18. S.G. Gorishny, A.L. Kataev, S.A. Larin, L.R. Surguladze, Mod. Phys. Lett. A **5** (1990) 2703; Phys. Rev. D **43** (1991) 1633; A.L. Kataev and V.T. Kim, Mod. Phys. Lett. A **9** (1994) 1309; L.R. Surguladze, Phys. Lett. B **338** (1994) 229, hep-ph/9406294; L.R. Surguladze, Phys. Lett. B **341** (1994) 60, hep-ph/9405325; K.G. Chetyrkin, Phys. Lett. B **390** (1997) 309, hep-ph/9608318; K.G. Chetyrkin, A. Kwiatkowski, Nucl. Phys. B **461** (1996) 3, hep-ph/9505358; S.A. Larin, T. van Ritbergen, J.A.M. Vermaseren, Phys. Lett. B **362** (1995) 134, hep-ph/9506465
19. A. Djouadi, J. Kalinowski, M. Spira, Comp. Phys. Comm. **108** (1998) 56, hep-ph/9704448
20. J. Gunion, H. Haber, G. Kane, S. Dawson, The Higgs Hunter's Guide, Addison-Wesley, 1990
21. S. Heinemeyer, W. Hollik, G. Weiglein, Comp. Phys. Comm. **124** (2000) 76, hep-ph/9812320
22. S. Heinemeyer, W. Hollik, G. Weiglein, Phys. Lett. B **455** (1999) 179, hep-ph/9903404
23. M. Carena, S. Mrenna, C. Wagner, Phys. Rev. D **60** (1999) 075010, hep-ph/9808312
24. M. Carena, S. Mrenna, C. Wagner, CERN-TH/99-203, hep-ph/9907422
25. H. Eberl, K. Hidaka, S. Kraml, W. Majerotto, Y. Yamada, HEPHY-PUB 729/99, hep-ph/9912463
26. M. Carena, D. Garcia, U. Nierste, C. Wagner, CERN-TH/2000-009, hep-ph/9912516
27. A. Djouadi, M. Spira, P.M. Zerwas, Z. Phys. C **70** (1996) 427, hep-ph/9511344
28. S. Heinemeyer, W. Hollik, Nucl. Phys. B **474** (1996) 32, hep-ph/9602318
29. A. Dedes, S. Heinemeyer, P. Teixeira-Dias, G. Weiglein, CERN-TH/99-368, hep-ph/9912249
30. W. Loinaz, J. Wells, Phys. Lett. B **445** (1998) 178, hep-ph/9808287
31. B. Allanach et al., Proceedings of UK Phenomenology Workshop on Collider Physics, Durham, UK, September 1999, hep-ph/9912302
32. R. Brinkmann et al. (editors), Conceptual Design of a 500 GeV e^+e^- Linear Collider with Integrated X-ray Laser Facility, DESY 97-048
33. S. Heinemeyer, W. Hollik, G. Weiglein, DESY 99-148, hep-ph/9910283
34. M. Carena, H. Haber, S. Heinemeyer, W. Hollik, C. Wagner, G. Weiglein, DESY 99-197, hep-ph/0001002